Interaction networks within biomolecular condensates feature topological cliques near the interface

Daniel Tan [1, *], Dilimulati Aierken [1, 2, *] and Jerelle A. Joseph [1, 2, †]

[1] *Department of Chemical and Biological Engineering, Princeton University, Princeton, NJ 08544, USA*
[2] *Omenn–Darling Bioengineering Institute, Princeton University, Princeton, NJ 08544, USA*

(Dated: March 25, 2025)

Biomolecular condensates are typically maintained by networks of molecular interactions, with canonical examples including those formed by prion-like low complexity domains (LCDs) of proteins. Single-component LCD condensates have been predicted to exhibit small-world network topologies and spatial inhomogeneities in protein compaction. Here, we systematically characterize molecular networks underlying condensates and investigate the relationship between single molecule properties and network topologies. We employ a chemically specific coarse-grained model to probe LCD condensates and generalize our findings by varying sequence hydrophobicity via a generic model that describes "hydrophobic–polar" (HP) polymers. For both model systems, we find that condensates are sustained by small-world network topologies featuring molecular "hubs" and "cliques". Molecular hubs with high network betweenness centrality localize near the centers of condensates and adopt more elongated conformations. In contrast, network cliques—densely interacting molecules that form locally fully connected subgraphs—are bridged by hubs and tend to localize near the condensate interface. Interestingly, we find power-law relationships between the structure and dynamics of individual molecules and network betweenness centrality, which describes molecular connectivity. Thus, our work demonstrates that inhomogeneities in condensate network connectivity can be predicted from single-molecule properties. Furthermore, we find that network cliques have longer lifetimes and that their constituent molecules remain spatially constrained, suggesting a role in shaping interface material properties.

Biomolecular condensates are liquid-like membraneless organelles inside living cells composed primarily of proteins and nucleic acids. Phase separation is a leading mechanism that accounts for condensate formation [1–4]. In this framework, proteins and nucleic acids demix from the cytosol or nucleoplasm, leading to two or more distinct liquid phases [5, 6]. Unlike simple liquids, evidence suggests that condensates are network fluids, where interactions between biomolecules can lead to the formation of percolated networks [7–11]. Indeed, governed by underlying networks of sequence-specific interactions, condensates display a wide range of viscoelastic behaviors [12–18]. Additionally, the viscoelasticity of condensates can evolve over time, leading to dynamically arrested states [17, 19–21]. While macroscopic features of condensates—such as varying viscoelasticity—have been observed, the underlying molecular networks that give rise to these behaviors remain poorly understood. Key questions remain: What are the characteristics of these molecular networks? How do they regulate the mesoscale organization of condensates? Can we predict network formation and structure from the properties of constituent biomolecules, or vice versa?

Intrinsically disordered regions (IDRs) are key components of proteins involved in phase separation and condensate formation [22]. Prion-like low-complexity domains (LCDs) are exemplary instances of IDRs in biomolecular condensation: LCD sequences contain repeat regions that serve as polymeric "spacers" and strongly interacting residues that act as "stickers" uniformly interspersed between spacer repeats [12, 23–27]. Percolated networks in LCD condensates are formed by the association of sticker residues along LCDs [9], and several recent studies have shown that condensates formed by proteins with LCDs are viscoelastic materials [11, 13, 14, 28, 29].

Through lattice simulation and graphical network analysis, Farag et al. first predicted the small-world network structure of molecular interactions in LCD condensates—highlighting inhomogeneities in the connectivity of networks underlying condensates [10]. These results were recently supported by experimental studies revealing inhomogeneous organizations of biomolecules in single-component LCD condensates [30]. Similar network analyses to Ref. 10 have been employed to probe molecular networks in two-component condensates [11], to determine the effect of temperature, length, and molecular sequence on networks underlying multicomponent condensates [31], and to study the effects of sequence patterning and binding affinities on percolation and phase separation [32]. Moreover, molecular simulations have predicted structural inhomogeneities of biomolecules within LCD condensates [10, 32–36]. Together, these studies suggest that inhomogeneities exist both in the network structures underlying condensates and in the properties of the individual constituent molecules.

The small-world network structure is a widely characterized graph-theoretic concept with many connections to biology [26, 37, 38]. Nodes (here, molecules) within small-world networks are closely connected. Moreover, this topology is marked by the presence of "hubs", a typically small subset of nodes that are central to the efficient connection of other nodes. Also present in such topologies are "cliques", locally fully- or densely-connected subgraphs of neighboring nodes that tend to be efficiently bridged to other neighborhoods

* These authors contributed equally
† Corresponding author: jerellejoseph@princeton.edu

via hubs. As a result, the small-world topology is inherently heterogeneous and imparts an uneven distribution of node roles. However, it remains unclear whether small-world network topologies are a general feature of condensates, what role such topologies play in organizing biomolecular condensates, and how network features relate to single-molecule characteristics.

Here, we systematically study the network topology of LCD condensates using a chemically-specific off-lattice coarse-grained model, Mpipi [39]. We also design a generic model of sticker–spacer heteropolymers to investigate the impact of sequence composition on network topology and probe the generality of our findings. We consistently find small-world interaction network topologies for both LCDs and generic heteropolymers. Surprisingly, we find that highly interacting clique molecules tend to localize near condensate interfaces. Furthermore, cliques exhibit longer lifetimes, suggesting a role in condensate aging, where pathological gelation and aggregation processes have been proposed to originate at the interface [19, 20, 40]. We further demonstrate that single-molecule structural characteristics can be predicted by molecular network properties. Notably, we find strong power-law relationships between node connectivity and molecular sizes and shapes in dense phases. Our work also predicts power-law relationships between single-molecule dynamics and node connectivity, revealing that cliques represent locally constrained sub-environments within condensates. Taken together, our results point to a strong relationship between network topology and molecular organization in LCD condensates, suggesting that networked interactions are critical for condensate organization, material properties, and function.

RESULTS

LCDs and sticker–spacer polymers form condensate-spanning interaction networks with small-world topologies

To investigate interaction networks underlying biomolecular condensates, we perform molecular dynamics (MD) simulations of single-component condensates (top panel in Fig. 1a). Here, we adopt Mpipi [39]—a chemically specific residue-resolution model that has been shown to describe well the phase behavior of disordered proteins—to probe LCD condensates. We also design an HP polymer model that describes hydrophobic ('H' or sticker) and hydrophilic ('P' or spacer) monomers [25, 41]. Using this latter approach, we systematically vary the fraction of stickers in the polymers to examine how well our findings for LCDs extend to generic sticker–spacer polymers.

In network representations of condensates, each individual molecule is represented as a node, and interacting nodes are connected with unweighted and undirected edges (bottom panel in Fig. 1a). Specifically, we assign edges between two interacting molecules (i.e., LCDs or HP polymers) A and B when the interaction potential energy $E_{AB} < -k_B T$, indicating stability of the interaction against thermal fluctuations.

Small-world networks are characterized by high clustering coefficients and low average shortest pathlengths between nodes [38, 42]. The extent to which networks are organized as small-world topologies is typically quantified through the estimators σ_{sw} and ω_{sw}, which are functions of the average clustering coefficient (C) and average shortest pathlength (L) between arbitrary nodes in the graph. The equations used to compute these graph parameters are described in the Methods. Values of $0 < \sigma_{sw} < 1$ indicate that clustering is low or average shortest pathlengths are long compared to equivalent Erdős–Rényi (ER) random graphs, and $\sigma_{sw} \approx 1$ indicates that the network is organized like an ER random graph. Characteristic small-world values $\sigma_{sw} > 1$ come from high clustering coefficients and average shortest pathlengths that are shorter than or comparable to those in ER random graphs. The second estimator ω_{sw} is bounded between -1 and 1, where $\omega_{sw} = -1$ corresponds to a regular, lattice-like graph structure and $\omega_{sw} = 1$ corresponds to a random-graph structure. The small-world region $\omega_{sw} \approx 0$ describes a graph structure that is both highly clustered—like regular lattices—and has short average path lengths, like ER random graphs [38, 43]. The balance of high clustering and short pathlengths underlies the small-world network's resilience and conduciveness to efficient, high-fidelity transfer: most nodes are well connected to local nodes in clustered "neighborhoods" (graph "cliques"), and these neighborhoods are globally connected through a small subset of highly connected "hub" nodes that effectively act as a "highway" mediating pairwise node relations through shortest paths.

As shown in Fig. 1b, all molecular interaction networks in LCD condensates exhibit small-world topologies, with characteristic $\sigma_{sw} > 1$ and $\omega_{sw} \approx 0$ values. These results are consistent with those from lattice simulations [10], where it was found that single-component A1-LCD condensates exhibit small-world topologies. All simulated LCDs have a fraction of aromatic "sticker" residues $f_h \approx 0.14$, which are distributed in a near-uniform pattern along the protein sequence. Thus, we perform simulations for HP polymers of length $N_{HP} = 150$ monomers with hydrophobicity $f_h = 0.14$. In addition, we also characterize systems with lower ($f_h = 0.02$) and higher ($f_h = 0.22$) hydrophobicities. Interestingly, the small-world topology still persists for generic HP polymers (Fig. 1b).

We also characterize the density of interaction graphs, which is described by the edge density ρ_{edge}. In particular, we can directly probe ρ_{edge} as a function of the fraction of hydrophobic monomers f_h using HP model systems. We find that as sequence hydrophobicity increases, HP model condensates form increasingly dense interaction graphs (Fig. 1c). This result is consistent with theoretical predictions for condensed associative polymers with distributed stickers [26, 44]. Notably, the HP sequence designed to reproduce the hydrophobicity of LCD sequences ($f_h = 0.14$) formed condensates with significantly denser interaction networks than those of LCDs. This likely occurs

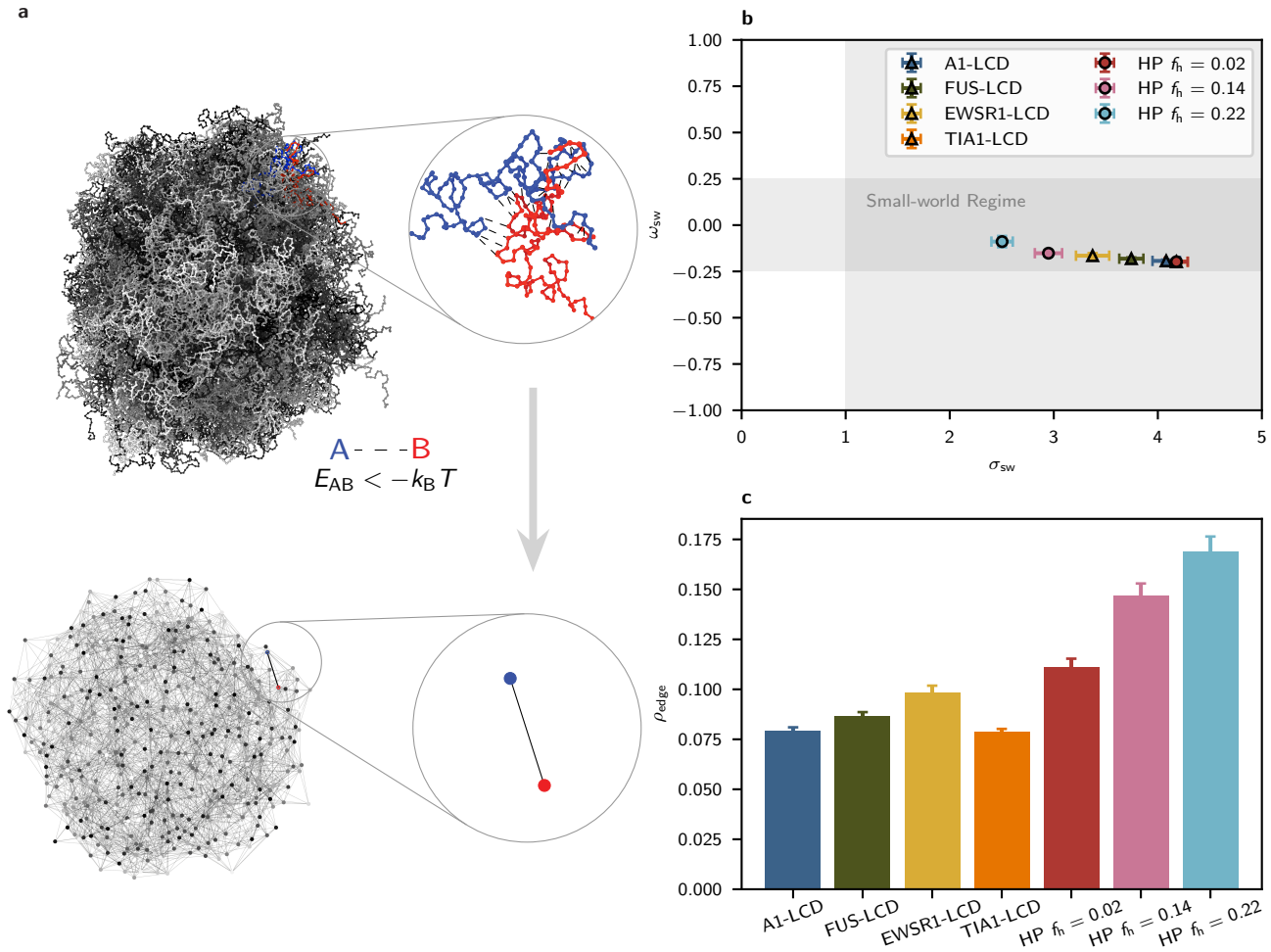

FIG. 1. **Small-world network structures are found for LCD and HP polymer condensates. a** Snapshot of a simulated condensate (top) and its corresponding graph representation (bottom), with two interacting molecules depicted in the insets. In the graph representation, each molecule is taken as a node, and two nodes are connected with an unweighted, undirected edge when the sum of pairwise monomer interaction energies (E_{AB}) between them exceeds the thermal energy ($k_B T$). **b** Small-world parameters σ_{sw} and ω_{sw} for single-component condensates of LCDs (triangles) and analog HP polymers (circles). Note that the average fraction of hydrophobic residues in the LCD sequences is $f_h(\text{LCD}) \approx 0.14$. A graph is considered small-world for $\sigma_{sw} > 1$ and $\omega_{sw} \approx 0$, and the gray shaded regions correspond to these respective regimes. **c** Average graph edge densities ρ_{edge} for simulated condensates, showing high variance in network connectivity and organization despite the conservation of small-world topological properties shown in b.

due to the weakly attractive P–P and H–P interactions in the HP model, a parameterization choice that reflects average non-sticker interaction statistics in Mpipi (described in the Methods). Due to averaging, the binary HP model does not fully capture the diverse physicochemical characteristics of LCD sequences—some of which promote repulsive residue–residue interactions that decrease interaction density.

Collectively, the conservation of small-world networks across biologically relevant LCDs and generic HP polymers suggests that these organizing principles contribute to the stability and function of condensates and likely phase-separated heteropolymers in general.

Molecular hubs and cliques are spatially segregated

To further characterize the molecular networks, we analyze the spatial distribution of small-world topological features within condensates. These topologies are marked by the presence of "hubs", which are members of a typically small subset of highly connective nodes. Hubs play critical roles in lowering average pathlengths by mediating many of the shortest paths connecting arbitrary node pairs. Small-world topologies also contain "cliques", locally fully-connected or densely-connected neighborhoods of nodes. In the context of biomolecular condensates, cliques indicate "subdomains" of closely interacting biopolymers. Clique substructures tend to be bridged to other cliques through network hubs, which promotes efficient flow and

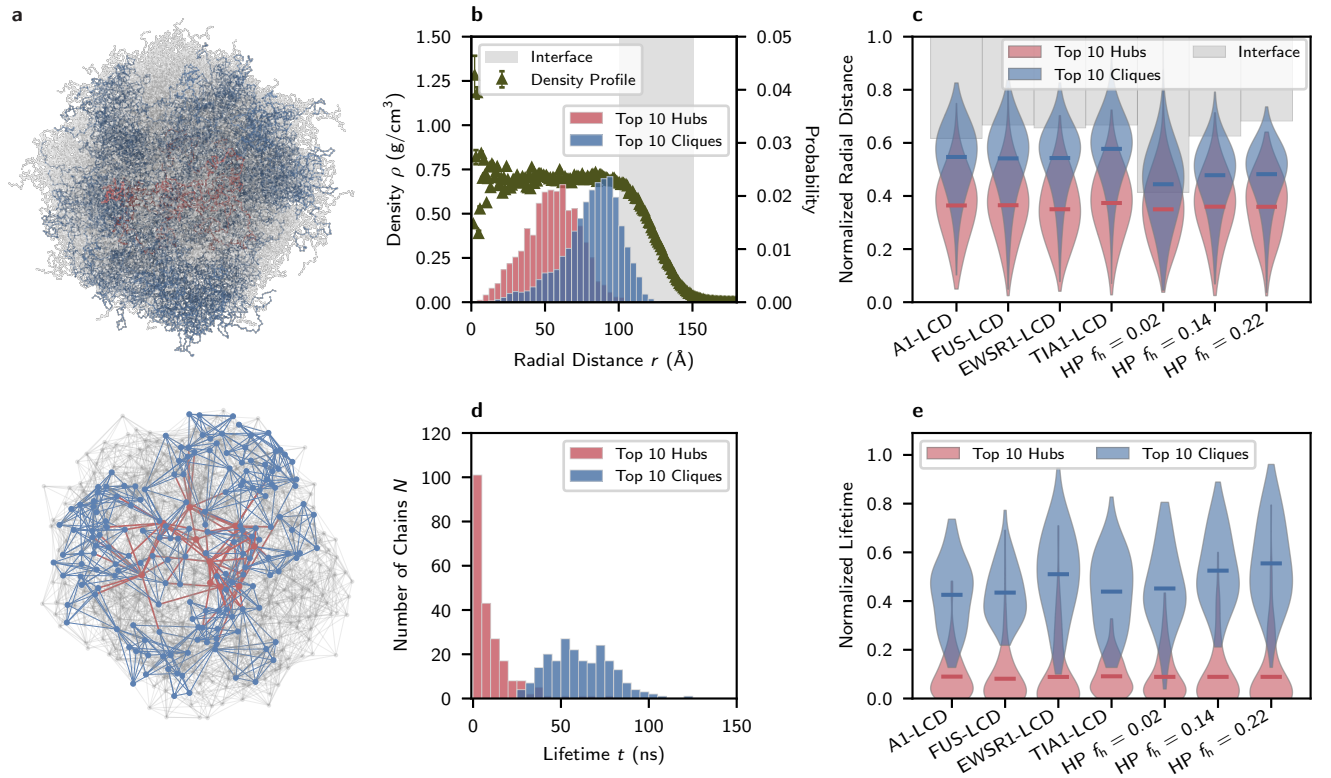

FIG. 2. **Network hubs and cliques are spatially and temporally distinct**. **a** Simulation snapshot and graph representation of an A1-LCD condensate (512 chains). Hubs are colored red and cliques are colored blue. Molecules colored gray are neither hubs nor members of the largest cliques. **b** Spatial distribution of hub molecules and clique molecules within a simulated FUS-LCD condensate (216 chains, $T = 270\,\mathrm{K}$). The clique molecules are closer to the interface than hub molecules. A radial distance of zero represents the center of mass of the condensate. The density profile is shown as triangles and the interface region is shaded in gray. An analogous profile from a simulation of 3375 FUS-LCD chains at $T = 300\,\mathrm{K}$ is shown in Supplementary Figure. S1; the observed distribution of hubs and cliques is persistent in larger systems and at higher temperatures. **c** The distribution of hubs and cliques for all simulated sequences in terms of normalized radial distance from the condensate center of mass. **d** The lifetime distribution of hub molecules and clique molecules are shown over 200 nanoseconds for FUS-LCD (216 chains, $T = 270$ K). Hub molecules are transient; the majority of hub molecules remain hubs on relatively short timescales while molecules within cliques remain members of cliques for substantially longer periods of time. **e** Normalized lifetimes of hub molecules and clique molecules are shown for all simulated sequences.

network resilience—both crucial properties of small-world topologies that drive their adoption in engineered and natural settings [45]. Interestingly, in our simulations, the largest cliques consistently comprised 7–8 nodes, suggesting that clique size may be determined by the valency of associative sites and by environmental conditions. To ensure that limits on clique sizes are not finite size effects, we simulate a large system with 3375 FUS-LCD chains and find that the largest clique size of 7–8 nodes is conserved even for very large condensates.

Beyond identifying small-world networks for the LCD and HP condensates, we examine the spatial distributions of both hub molecules and clique molecules. The typical distributions of hub and clique molecules in both real space (Fig. 2a, top panel) and in the graph representation (Fig. 2a, bottom panel) are depicted. Hubs are identified by high betweenness centralities C_B, a measure of the extent to which a single node "controls" shortest paths between arbitrary node pairs in the graph. Detailed calculations are shown in the Methods. Here, the top 10 hub molecules (i.e., highest betweenness centrality C_B) are colored in red and the 10 largest cliques are shown in blue. Strikingly, in both visual representations, it is immediately clear that hubs and cliques occupy distinct spatial regions. We further quantify the spatial distribution of hubs and cliques in the condensates. As shown for simulations of FUS-LCD in Fig. 2b, the density profile is roughly uniform within the condensate, featuring a well-defined interface that indicates the stability of this thermodynamic quantity. However, despite this homogeneous density profile, the distributions of hub molecules and clique molecules are distinctly heterogeneous. More specifically, cliques are located closer to the interface than are hubs. We further confirm that such distributions are not a special case for FUS-LCD but are generic features of LCD and HP condensates, as characterized in Fig. 2c.

Additionally, we find that the spatial distributions of hubs and cliques are dependent on sequence hydrophobicity. Specifically, we probe this behavior among the HP

sequences. At low sequence hydrophobicity ($f_h = 0.02$), the spatial separation between hubs and cliques is found to be minimal, and the phase interface housed a substantive fraction of molecular hubs and cliques. This suggests that as polymer sequences become more homogeneous, interaction network structures themselves become more homogeneous. At high sequence hydrophobicity ($f_h = 0.22$), hubs and cliques remain spatially distinct; however, all of the largest cliques are completely localized prior to the phase interface, indicating that these regions are more shielded from the solvent.

Together, we find that the valency of associative residues in LCDs and HP sequences enables the formation of condensate-spanning small-world interaction networks. Further, hubs and cliques within condensates correspond to distinct spatial regimes of molecular interactivity.

Molecular hubs and cliques exhibit distinct lifetimes

We also analyze the lifetimes of hubs and cliques within condensates composed of LCDs and HP polymers (see Methods). Here, we measure molecular lifetimes based on their network identities: we quantify how long a molecule is continuously identified as a hub or as belonging to a clique. For FUS-LCD, we find that cliques exhibit significantly longer lifetimes than hubs (Fig. 2d). In fact, for all LCDs probed, individual molecules very scarcely serve as connective hubs for more than 1–2 ns in our simulations, while members of cliques remain in those cliques for substantially greater time fractions (Fig. 2e). This clear temporal separation of hubs and cliques is also observed for HP model sequences (Fig. 2e). Though hubs generally have shorter lifetimes, we find that as sequence hydrophobicity increases, a small fraction of hubs exhibit longer lifetimes (see tails of distributions for HP polymers in Fig. 2e). Moreover, higher sequence hydrophobicity also leads to longer molecular lifetimes within cliques, aligning with recent experiments for single-component condensates formed by aromatic mutants of A1-LCD [30].

For LCD sequences, we find that the lifetimes of cliques are dependent on sequence length and diversity (Fig. 2e)—effects not captured in the binary HP sequences. For example, EWSR1, the longest LCD tested, exhibits longer clique lifetimes compared to other LCDs; TIA1, the most hydrophobic LCD tested, exhibits a broader distribution of clique lifetimes compared to the other LCDs. Our results suggest that distinctions between hub and clique lifetimes may be universal features of LCD condensates.

Molecular conformational properties are power laws of node betweenness centrality

Recent work has reported heterogeneous conformational ensembles of disordered proteins within condensates. In particular, proteins exhibit key differences in average molecular size (i.e., radius of gyration R_g), which have been reported for proteins at the interface versus those in the condensate core [10, 34, 36]. At the same time, graph theory has been applied to reveal inhomogeneities in molecular connectivity within condensates [10, 11, 30–32]. Given the distinct topological features—hubs and cliques—in networks underlying LCD and HP-polymer condensates, we investigate whether strong relationships exist between single-molecule characteristics and network properties (Fig. 3a) in these systems. Specifically, for LCD and HP systems, we measure the radius of gyration R_g and shape anisotropy κ^2 of polymers in the condensates. R_g provides insight into the average molecular size, while κ^2 effectively describes the deviation of polymer shape from a perfect sphere [46–48] (Fig. 3b).

We first compare single-molecule R_g (normalized by the maximum length of a linear chain; see Methods) against molecular betweenness centrality C_B (normalized; see Methods). Recall that C_B quantifies the importance of a molecule (i.e., node) in terms of how often it appears on the shortest paths between other molecules. We find that R_g versus C_B in $\log_{10}$–$\log_{10}$ space yields a positive linear relationship (Fig. 3c), indicating a consistent power law behavior:

$$R_g = aC_B^k \rightarrow \log_{10}(R_g) = b + m\log_{10}(C_B). \quad (1)$$

To further quantify this relationship, we utilize $b = \log_{10}(a)$ and $m = k$ to perform a linear fit in $\log_{10}$–$\log_{10}$ space. The dependence of b and m on the length of LCD sequences is shown in Fig. 3d. The marginal increase in m shows strong positive correlation with the chain length. The increase of m (i.e., exponent k) with chain length suggests a stronger dependence of R_g on C_B for longer LCDs. In general, molecular valency increases with chain length, meaning molecules on average can form more favorable intermolecular interactions in the condensate environment. In this scheme, bridging more molecules (higher C_B) yields larger structures (larger R_g).

In contrast, we find that the prefactor b is strongly negatively correlated with the chain length (Fig. 3d). We reason that the unexpected decrease in b (i.e. prefactor a) with increasing chain length is an artifact of the R_g normalization scheme employed. Indeed, when we plot the data in linear space instead of $\log_{10}$–$\log_{10}$ space, longer chains demonstrate both an R_g curve with a greater asymptote and a prefactor that scales linearly with chain length.

We also assess the scaling relationship between R_g and C_B for fixed-length HP sequences (Fig. 3c,e). Here, we find that both the scaling exponent m and the prefactor b are strongly positively correlated with the hydrophobicity f_h (Fig. 3e). This result indicates that as chain hydrophobicity increases, inter-chain interactions become more favorable—reflected by higher C_B and R_g. Increases in chain hydrophobicity lead to more hydrophobic condensate interiors, and the favorable "molecular solvent" environment in the dense phase supports chain expansion by strengthening the preference for inter-chain interaction.

Similar to R_g, the molecular relative shape anisotropy κ^2 is also found to follow power-law relationships with molecular C_B (Fig. 3f). κ^2 is a scale-invariant quantity, ranging from $\kappa^2 = 0$ at the limit where polymers adopt a spheri-

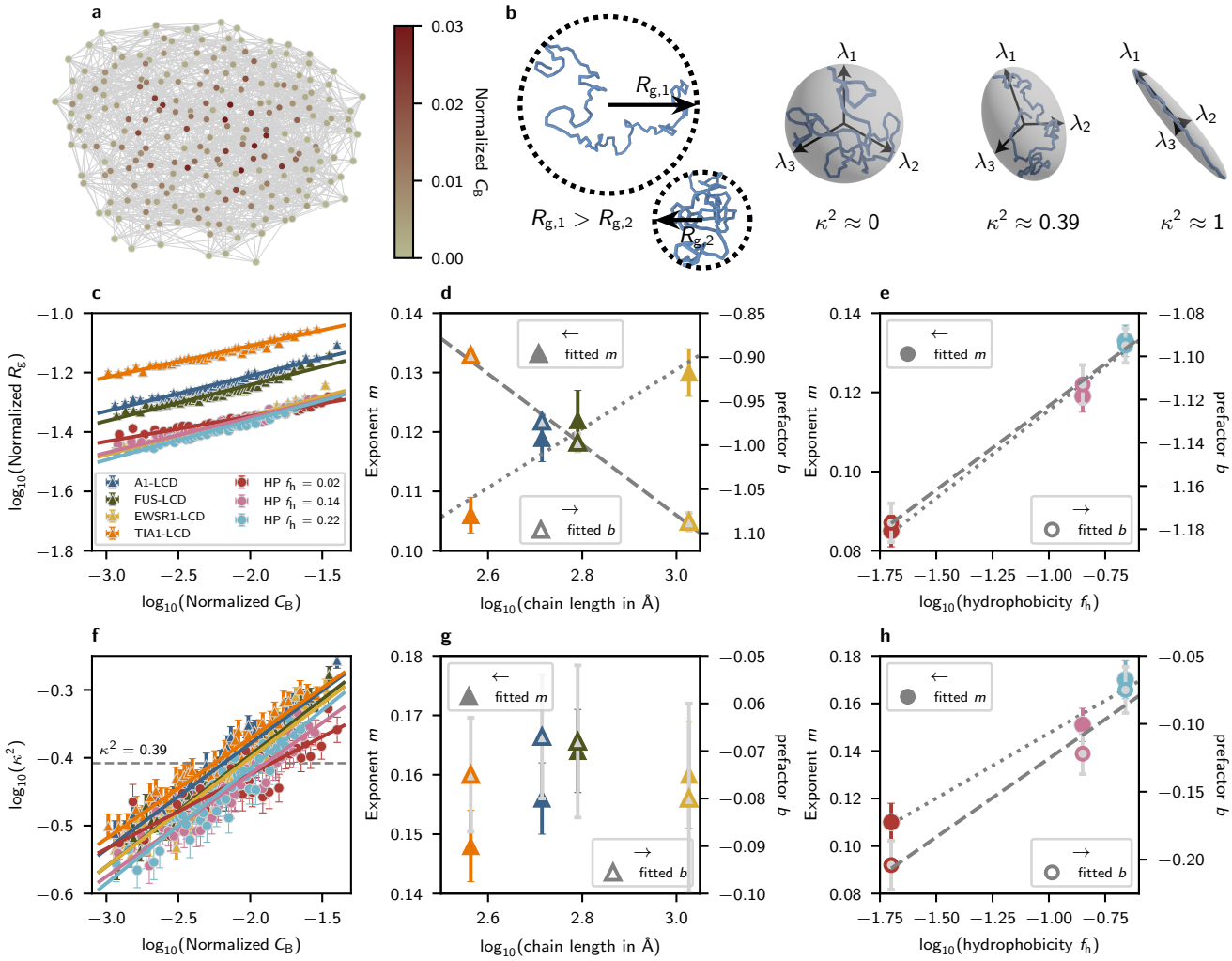

FIG. 3. **Single-chain radius of gyration R_g and shape anisotropy κ^2 follow power-law relationships with molecular connectivity in interaction networks.** **a** A graph of an A1-LCD condensate. Nodes are colored based on their betweenness centrality C_B. **b** (left) Schematic representations of chain radius of gyration R_g. (right) Schematic representations of the eigenvectors λ of the gyration tensor and values of the scale-invariant shape anisotropy parameter κ^2 for distinct chain conformations. $\kappa^2 = 0$ represents a perfect, radially isotropic sphere, $\kappa^2 \approx 0.39$ corresponds to an ideal-chain conformation, and $\kappa^2 = 1$ describes a perfectly anisotropic elongated chain. **c** All simulated sequences display power-law relations between the betweenness centrality C_B and radius of gyration R_g, indicated by linear fits in $\log_{10}$–$\log_{10}$ space. **d** The relationship between LCD chain length and linear fit parameters for the $\log_{10}$–$\log_{10}$ plots in c. Two-parameter $R_g = aC_B^k$ power-law fits are performed for $m = k$ and $b = \log_{10}(a)$. **e** The relationship between HP polymer hydrophobicity and linear fit parameters for the $\log_{10}$–$\log_{10}$ plots in c. The same two-parameter fitting is employed as in d. **f** All simulated sequences display power-law relations between the betweenness centrality C_B and relative shape anisotropy κ^2. **g** Power-law fit parameters for different LCD chain lengths using a two-parameter power law $\kappa^2 = aC_B{}^k$ for the $\log_{10}$–$\log_{10}$ plots in f, analogous to d. **h** Power-law fit parameters for different sequence hydrophobicities in f.

cally isotropic conformation to $\kappa^2 = 1$ at the limit where they are completely linear (Fig. 3b). Previous simulation studies have reported the average relative shape anisotropy of individual polyampholytes in condensed phases [34], with dense-phase κ^2 consistently between 0.42 and 0.44 invariant to changes in sequence. Compared to an ideal-chain $\kappa^2 =$ 0.39, LCD/HP molecules with low C_B adopt slightly collapsed, globular conformations ($\kappa^2 \approx 0.28$), while the highly connected hublike molecules are extended ($\kappa^2 \approx 0.48$).

We find that hublike character is synonymous with stretched, elongated conformations, where transient interchain interactions serve to randomly reorient and extend the molecule. Though macromolecular densities in condensates appear uniform (Fig. 2b), these results suggest that physicochemical environments inside condensates may not be. No significant correlations are found between κ^2 power law parameters and chain length (Fig. 3g). In contrast, increased sequence hydrophobicity leads to greater exponents

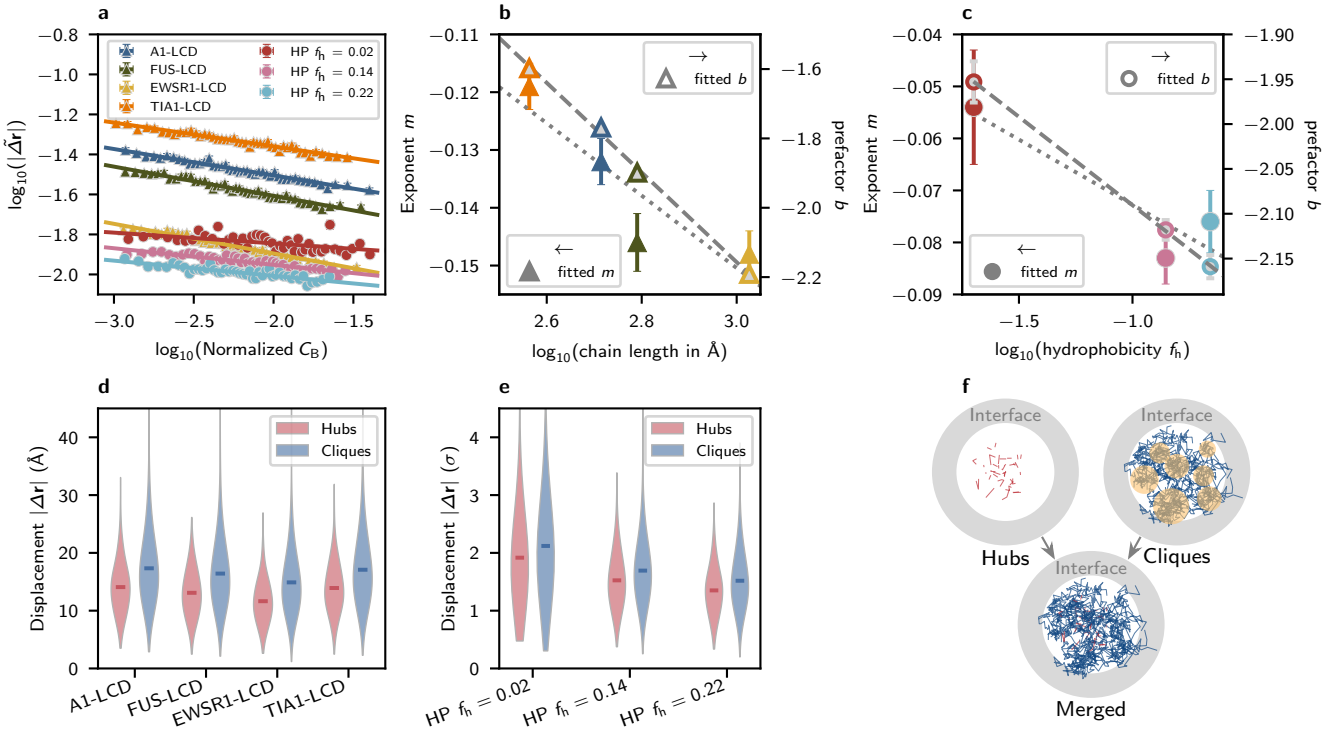

FIG. 4. **Dynamics of molecules within single-component condensates is correlated with network topological organization.** **a** Normalized instantaneous displacements $|\tilde{\Delta \mathbf{r}}|$ of single chains in condensed phases exhibit strong negative correlations with node betweenness centrality C_B within molecular graphs. LCD sequences are simulated at $T = 270$ K and HP sequences at $T^* = 0.5\, k_B T/\epsilon$. **b** Plots of the parameters of the linear fits to the LCD data in $\log_{10} - \log_{10}$ space in a, as a function of sequence length. **c** Plots of the parameters of the linear fits to $\log_{10} - \log_{10}$ HP data in a, as a function of sequence hydrophobicity with fixed sequence length ($n_{HP} = 150$). **d** Displacements within consistent time intervals are compared for hub molecules and clique molecules in LCD condensates. **e** Displacements within consistent time intervals are compared for hub molecules and clique molecules in HP polymer condensates. **f** A 2-dimensional visualization of the trajectories of hub molecules (red) and clique molecules (dark blue) in a FUS-LCD condensate, plotted as lines when their hub or clique-member status is contiguous in time. The phase interface is shown as a gray circular band. Locally confined regions of clique molecules are indicated by yellow circles.

and prefactors (Fig. 3h), further suggesting that the condensate environment becomes a better solvent for polymers with increasing sequence hydrophobicity.

Dynamics of molecules in biomolecular condensates are dependent on network topology

In addition to characterizing the variance in molecular structures within condensates, another property of interest is the dynamics of individual molecules. In particular, we investigate scaling relationships between the displacement of molecular centers of mass ($|\Delta \mathbf{r}|$) and betweenness centrality (C_B). The computation and normalization of these quantities are described in the Methods.

Similar to the conformational properties R_g and κ^2, we find that normalized molecular displacement $|\tilde{\Delta \mathbf{r}}|$ follows a power-law relationship with C_B in $\log_{10}$–$\log_{10}$ space (Fig. 4a). Moreover, both the prefactor and the exponent decrease as LCD length increases (Fig. 4b), or as sequence hydrophobicity increases (Fig. 4c). These results are intuitive: longer polymers and/or polymers with more associative interactions exhibit reduced molecular motion within condensates.

Experimental and simulation studies have characterized the diffusion of LCDs within condensates [49, 50]. More recent experimental studies have shown that FUS–RNA condensates contain "nanodomains", locally densely connected substructures that decrease local diffusivity in the dense phase without a secondary phase separation [51]. To study this effect, we analyze the local movements of hub and clique molecules in our systems. On short timescales, the displacements of clique molecules are consistently greater than those of hubs (Fig. 4d,e). When combined with our previous analysis, which reveals that cliques have longer lifetimes (Fig. 2d,e), we conclude that the "faster" motion of clique molecules is best described as a form of local vibration. Indeed, when we trace the displacement of molecules in cliques and hubs, the motion of clique molecules is highly localized (see the 2D projections of molecular motion in Fig. 4f). Thus, while cliques experience relatively larger displacements than hubs, these displacements remain lo-

calized. Such confinement of clique motion is reminiscent of the nanodomains described in Ref. 51, as well as of recent experiments reporting highly interactive hydrophobic "hotspots" in A1-LCD condensates [30].

DISCUSSION

Macroscopically, condensates often appear as homogeneous structures in both experimental and simulated reconstitution. However, evidence suggests that even single-component condensates can exhibit inhomogeneities in their microstructure [10–12, 26, 30]. Importantly, the molecular networks underlying condensates play a crucial role in shaping their material properties and functions. Thus, understanding how molecules organize within condensates to encode mesoscale properties is an emerging area in the field.

In this work, we leverage residue-resolution molecular dynamics simulations alongside graph theory to characterize the molecular networks of condensates formed by the low-complexity domains (LCDs) of key phase-separating proteins (hnRNPA1, FUS, EWSR1, and TIA1). To assess the generality of our findings, we also characterize condensate systems composed of sequences with varying fractions of hydrophobic (H) and polar (P) monomers. These HP systems represent heteropolymers with varying propensities for forming percolated networks within condensates. Consistent with previous lattice-based simulations of A1-LCD [10], we find that both biological LCDs and generic HP polymers form small-world interaction network topologies.

Small-world networks contain two major topological features, "hubs" and "cliques". Cliques are densely connected groups of nodes (here, molecules) representing fully connected subgraphs within the network. The cliques themselves are efficiently connected through hub nodes, which reduce average shortest path lengths between arbitrary node pairs in the network. Notably, we find that hubs are positioned closer to the condensate center, while the largest cliques are located near the interface. These observations hold for all biological LCDs and HP sequences studied in this work. In addition to the spatial distinction observed between hubs and cliques, we find that hub molecules and clique molecules have distinct lifetimes: the molecular identities of connective hubs change rapidly, while members of cliques tend to remain in those cliques over longer timescales due to the formation of stable, fully-connected subnetworks.

Given that LCD condensates exhibit small-world topologies with heterogeneous molecular connectivities, we also show that molecular conformations and connectivities within interaction networks are highly correlated. Interestingly, the radius of gyration (i.e., average size) and shape anisotropy (i.e., ranging from spherical to linear) of individual molecules are found to be power laws of molecular betweenness centrality (i.e., connectivity) within interaction networks. We further explored how the power law prefactors and exponents are regulated by molecular chain length and sequence hydrophobicity. We find a close similarity in the exponents across simulated systems, suggesting the potential existence of a universal exponent for such relationships in LCD condensates. However, limited data and flexibility inherent in two-parameter fitting prevent us from drawing definitive conclusions in this regard.

In addition to structural properties of molecules, we also explored their dynamics within interaction networks. We find that molecules become less dynamic as their betweenness centrality increases. This result is intuitive as more expanded molecules with larger betweenness centralities are subject to greater confinement through dense intermolecular interactions in the condensate environment. Interestingly, this relationship also shows power-law behavior. To our surprise, molecules in cliques exhibit slightly faster motions than hub molecules. However, explicitly tracing their trajectories reveals that clique molecules are spatially confined. This suggests that their movement is primarily characterized by local vibrations, whereas hub molecules exhibit motion across larger regions.

A key limitation of this work is that the probed condensates are composed solely of disordered protein sequences that engage in transient interactions. In contrast, cellular condensates often include both disordered and structured components that dictate their form and function [52]. The latter can mediate long-lived, high-affinity interactions that shape the underlying interaction networks, as recent studies suggest [53, 54]. Exploring systems with specific binding interactions—such as those involving folded protein domains or RNA—would therefore be an important next step. Nonetheless, our findings show that even simple systems of disordered protein regions exhibit striking microstructural inhomogeneities and complex biophysical behaviors.

Collectively, our results suggest a framework in which LCDs form inhomogeneous molecular networks in condensates. Notably, molecular networks contain topological cliques that represent fully connected groups of molecules. Recent experiments have reported highly interactive hydrophobic nanoclusters in A1-LCD condensates [30]. Although Ref. [30] refers to these regions as "hubs," their nanoclusters align with the "cliques" found in our systems according to graph-theoretic frameworks. Other work on multicomponent condensates has also identified nanodomains within condensates [51], which appear to be consistent with the cliques we observe in LCD and HP polymer condensates. Alongside these studies, experiments report that pathological liquid-to-gel transitions in condensates originate at their interfaces [19, 40]. Additionally, the formation of interfacial aggregates resembling amyloid fibrils were observed in the early stages of FUS condensate aging [20, 40]. Thus, we hypothesize that the presence of locally constrained, highly interacting molecules (cliques) near the condensate interface, as observed in our simulations, may lead to the formation of more stable, longer-lasting associations over time, ultimately influencing the material properties of condensate interfaces.

METHODS

In this work, we study the single-chain characteristics and interaction network topologies of condensates formed by prion-like low-complexity domains (LCDs) using Mpipi—a residue-level coarse-grained model for disordered proteins [39]. We further study interaction networks of condensates via a generic model of heteropolymers, the binary HP model. In the HP polymer simulations, we systematically vary sequence hydrophobicity to investigate its impact on the topology of emergent interaction networks.

1. LCD and HP sequences

We use the Mpipi model [39] to simulate four biological phase-separating protein sequences: the low-complexity domain of the human ribonuclear protein hnRNPA1 (A1-LCD), the low-complexity domain of the Fused in Sarcoma protein (FUS-LCD), the low-complexity domain of the RNA-binding protein EWS (EWSR1-LCD), and the low-complexity domain of the T-cell intracellular antigen 1 (TIA1-LCD). These LCDs are marked by a sequence distribution overrepresented in Glutamine (Q), Serine (S), Glycine (G), and Tyrosine (Y) residues. The polar uncharged residues Q, S, and G act as weakly interactive "spacers" along sequences, serving to segregate highly attractive "sticker" residues (particularly Y) uniformly along the sequence. TIA1-LCD also incorporates tryptophan (W) residues along the sequence that can enable "sticky" interactions with itself and tyrosine (Y) through π–π stacking of aromatic rings.

A1-LCD
GSMAS ASSSQ RGRSG SGNFG GGRGG GFGGN
DNFGR GGNFS GRGGF GGSRG GGGYG GSGDG
YNGFG NDGSN FGGGG SYNDF GNYNN QSSNF
GPMKG GNFGG RSSGG SGGGG QYFAK PRNQG
GYGGS SSSSS YGSGR RF

EWSR1-LCD
MASTD YSTYS QAAAQ QGYSA YTAQP TQGYA
QTTQA YGQQS YGTYG QPTDV SYTQA QTTAT
YGQTA YATSY GQPPT GYTTP TAPQA YSQPV
QGYGT GAYDT TTATV TTTQA SYAAQ SAYGT
QPAYP AYGQQ PAATA PTRPQ DGNKP TETSQ
PQSST GGYNQ PSLGY GQSNY SYPQV PGSYP
MQPVT APPSY PPTSY SSTQP TSYDQ SSYSQ
QNTYG QPSSY GQQSS YGQQS SYGQQ PPTSY
PPQTG SYSQA PSQYS QQSSS YGQQS SFRQD
HPSSM GVYGQ

FUS-LCD
MASND YTQQA TQSYG AYPTQ PGQGY SQQSS
QPYGQ QSYSG YSQST DTSGY GQSSY SSYGQ
SQNTG YGTQS TPQGY GSTGG YGSSQ SSQSS
YGQQS SYPGY GQQPA PSSTS GSYGS SSQSS
SYGQP QSGSY SQQPS YGGQQ QSYGQ QQSYN
PPQGY GQQNQ YNS

TIA1-LCD
MINPV QQQNQ IGYPQ PYGQW GQWYG NAQQI
GQYMP NGWQV PAYGM YGQAW NQQGF NQTQS
SAPWM GPNYG VQPPQ GQNGS MLPNQ PSGYR
VAGYE TN

As for the minimal HP model, we simulate chains with a constant length $n = 150$ to be close to the length of the LCD sequences described above. Furthermore, three sequence variants with hydrophobic fractions $f_h = 0.02, 0.14, 0.22$ are simulated and analyzed. These values correspond to chains that are "as sticky" as the LCDs ($f_h \approx 0.14$), significantly less sticky than the LCDs ($f_h = 0.02$), and more sticky than the LCDs ($f_h = 0.22$). Analogous to LCD architectures, each constructed variant distributes $f_h \times n$ hydrophobic (H) beads as evenly as possible along the sequence.

HP ($f_h = 0.02$)
PPPPP PPPPP PPPPP PPPPP PPPPP HPPPP
PPPPP PPPPP PPPPP PPPPP PPPPP PPPPP
PPPPP PPPPP PPPPP HPPPP PPPPP PPPPP
PPPPP PPPPP PPPPP PPPPP PPPPP PPPPP
PPPPP HPPPP PPPPP PPPPP PPPPP PPPPP

HP ($f_h = 0.14$)
PPPHP PPPPP HPPPP PPHPP PPPPH PPPPP
PHPPP PPPHP PPPPP HPPPP PPPHP PPPPP
HPPPP PPHPP PPPPH PPPPP PHPPP PPPHP
PPPPP HPPPP PPPHP PPPPP HPPPP PPHPP
PPPPH PPPPP PHPPP PPPHP PPPPP HPPPP

HP ($f_h = 0.22$)
PPHPP PPHPP PHPPP PHPPP HPPPP HPPPH
PPPPH PPPHP PPPHP PPHPP PPHPP PPHPP
PHPPP PHPPP HPPPP HPPPH PPPPH PPPHP
PPPHP PPHPP PPHPP PPHPP PHPPP PHPPP
HPPPP HPPPH PPPPH PPPHP PPPHP PPHPP

2. Mpipi model

In Mpipi, each protein residue is represented by a single interaction site/bead. Each bead has an assigned mass, charge, molecular diameter, and other interaction parameters. The potential energy in the Mpipi model is taken as the sum of bonded and non-bonded interaction terms.

$$E_{\text{Mpipi}} = E_{\text{bond}} + E_{\text{elec}} + E_{\text{pair}}. \tag{2}$$

Specifically, beads are bonded via harmonic springs.

$$E_{\text{bond}} = \sum_i \frac{1}{2} k (r_i - r_{0i})^2, \tag{3}$$

Non-bonded interactions encompass long-ranged electrostatics, which are captured via a Coulomb term with Debye–Hückel screening,

$$E_{\text{elec}} = \sum_{i,j} \frac{q_i q_j}{4\pi\epsilon_r\epsilon_0 r_{ij}} \exp(-\kappa r_{ij}), \tag{4}$$

and short-ranged pairwise contacts, which are modeled via the Wang–Frenkel potential [55],

$$E_{\text{pair}} = \sum_{i,j} \varepsilon_{i,j}\alpha_{i,j} \left[\left(\frac{\sigma_{i,j}}{r}\right)^{2\mu_{i,j}} - 1\right] \left[\left(\frac{r_c}{r}\right)^{2\mu_{i,j}} - 1\right]^{2\nu_{i,j}}. \tag{5}$$

All model parameters are discussed in detail in Refs. 39 and 27 and are provided in our GitHub repository (see Data Availability Statement). In Mpipi, the solvent is modeled implicitly, and the model was parameterized by combining bioinformatics data and atomistic potentials-of-mean force calculations. Previous work has demonstrated that Mpipi accurately captures both single-chain properties and collective phase behaviors of disordered proteins [27, 39, 56].

3. HP model parameterization

The binary HP model is designed to approximate LCD interactions in condensates by representing LCDs as sticker–spacer associative polymers. The HP model consists of two bead types: hydrophobic (H) and polar (P), both with radius σ. H beads are used to represent stickers while P beads are weakly associative residues acting as spacers between hydrophobic residues. A sequence's hydrophobicity fraction f_h, or its "stickiness," is determined as the number of hydrophobic residues divided by the length of the sequence. The total interaction energy E_{HP} consists of contributions from nonbonded pairwise interactions $E_{pair,HP}$ and bonded interactions $E_{bond,HP}$:

$$E_{HP} = E_{pair,HP} + E_{bond,HP}. \tag{6}$$

The pairwise monomeric interactions between beads i and j are described by a Lennard-Jones (LJ) potential

$$E_{pair,HP}(r_{ij}) = \begin{cases} 4\epsilon_{ij}\left[\left(\frac{\sigma}{r_{ij}}\right)^{12} - \left(\frac{\sigma_{ij}}{r_{ij}}\right)^{6}\right], & r \le 3\sigma, \\ 0, & \text{otherwise.} \end{cases} \tag{7}$$

Here, r_{ij} represents the distance between beads i and j, each of which may be of type H or P. All the beads are set to have the same size σ and same mass m. The H–H pairwise interaction is set to $\epsilon_{HH} = 1.0$. Other interaction strengths ϵ_{HP} and ϵ_{PP} are determined by normalizing and rescaling the Mpipi interaction strengths. In the Mpipi model, the average of strong interaction strengths encoding π–π and cation–π pairwise interactions (e.g., YY, FF, FY, RY...) is

$$\langle \epsilon_{YFWR,Mpipi} \rangle = 1.948\,\text{kJ/mol}, \tag{8}$$

while the average of other interactions is

$$\langle \epsilon_{else,Mpipi} \rangle = 0.349\,\text{kJ/mol}. \tag{9}$$

Finally, the weakly associating H–P and P–P interactions are determined by rescaling against the H–H interaction strength:

$$\epsilon_{HP,PP} = \frac{\langle \epsilon_{else,Mpipi} \rangle}{\langle \epsilon_{YFWR,Mpipi} \rangle} \times \epsilon_{HH} = 0.179\,\epsilon_{HH}. \tag{10}$$

The bonded interactions in the HP model are modeled by the finite extensible nonlinear elastic (FENE) bond potential [57]:

$$\begin{aligned} E_{bond,HP}(r_{i,i+1}) = &-\frac{1}{2}KR_0^2 \ln\left[1 - \left(\frac{r_{i,i+1}}{R_0}\right)^2\right] \\ &+ 4\epsilon_{bond}\left[\left(\frac{\sigma_{bond}}{r_{i,i+1}}\right)^{12} - \left(\frac{\sigma_{bond}}{r_{i,i+1}}\right)^{6}\right] \\ &+ \epsilon_{bond} \end{aligned} \tag{11}$$

where $r_{i,i+1}$ is the bond length of the ith bond, the spring constant is set to $K = 30\,\epsilon_{HH}/\sigma^2$, the maximum bond length is $R_0 = 1.5\,\sigma$, and the repulsive Lennard-Jones terms are set to $\epsilon_{bond} = \epsilon_{HH}$ and $\sigma_{bond} = \sigma$.

4. Molecular dynamics simulations

Implicit-solvent simulations of all single-component LCD and HP model systems are conducted in the NVT ensemble using the LAMMPS package [58].

LCD simulations are prepared with an initial density of $\rho = 0.05\,\text{g/cm}^3$ at $T = 270\,\text{K}$ and $T = 310\,\text{K}$ in an isotropic cubic box with periodic boundary conditions, and NPT simulations were performed to accelerate the condensate formation process during the initial steps. The integration timestep is set to $dt = 10\,\text{fs}$, and systems are simulated for $1\,\mu\text{s}$ after condensate formation for equilibrium sampling. 1000 frames are sampled uniformly along equilibrium trajectories for each LCD sequence. Results from both temperatures are consistent; results from simulations at $T = 270\,\text{K}$ are shown in the main text. At this temperature, all systems are below their critical points, enabling direct comparison.

HP simulations are performed with the same steps as LCD sequences with a integration timestep $d\tau = 0.005\sqrt{m\sigma^2/\epsilon}$ at $T^* = 0.5\,k_B T/\epsilon_{HH}$. Production runs for each HP sequence are performed for $10^8 d\tau$, and 1000 trajectory frames are sampled uniformly as in the LCD simulations. For each sampled frame in both simulation types, dense-phase centers of mass and single-molecule conformations are obtained using OVITO [59].

5. Construction of interaction graphs

Interaction matrices representative of single static frames are constructed from particle position data, and we use an energetic criterion to ensure that the interaction energy of two chains a and b exceeds the thermal energy, i.e., $E_{pair,ab} < -k_B T$, when recording an interaction. For N condensed polymers, a 2-dimensional interaction matrix (adjacency matrix) $M = N \times N$ is constructed, where M_{ab} is assigned as follows:

$$M_{ab} = \begin{cases} 1, & \sum_{i,j} E_{pair}(r_{ij}) \le -k_B T, \\ 0, & \text{else.} \end{cases} \tag{12}$$

Here i and j index over each bead (residue/monomer) along respective protein chains a and b, and r_{ij} is the distance between monomers a and b. Finally, graph structures are generated with the NetworkX python package [60] using binary interaction matrices as adjacency matrices M. Each node in a frame's representative graph represents a single protein chain, and unweighted, undirected edges are drawn between nodes if an attractive interaction between them is observed in that frame according to the above criteria.

Interaction networks are studied for small-world-like topologies by finding node betweenness centralities C_B and calculating the small-world coefficients σ_sw and ω_sw [38, 43, 61]. The betweenness centrality C_B of a node i is found and normalized via the NetworkX `betweenness_centrality()` utility and is computed as follows:

$$C_\mathrm{B}(i) = \frac{2}{(N-1)(N-2)} \sum_{i \neq s \neq t} \frac{\ell_{st}(i)}{\ell_{st}}, \tag{13}$$

where the pair (s,t) enumerates over all node pairs in the graph (excluding i), ℓ_{st} is the total number of shortest paths between s and t, and $\ell_{st}(i)$ is the number of shortest paths that flow through node i. The normalization coefficient is the inverse of the binomial coefficient $\binom{N-1}{2}^{-1} = 2/[(N-1)(N-2)]$ for a graph with $N-1$ nodes, enumerating over all combinations of node pairs excluding i. Betweenness centralities are normalized to facilitate comparison between graphs of systems of differing sizes, as the summation suggests that it is a metric that scales with the number of nodes N.

Graphs are generally considered to have small-world topologies if neighbors of any given node are highly connected to each other, if shortest pathlengths between any given pair of nodes are low, and if the graph is sparse [38]. Both σ_sw and ω_sw serve as estimators of the "small-worldness" of a given graph by comparing its average shortest pathlength $L = \langle \ell_\mathrm{min} \rangle$ and its average clustering coefficient C to the same quantities C_rand and L_rand found for a series of Erdös–Rényi random graphs, and C_latt and L_latt for equivalent lattice graphs :

$$\sigma_\mathrm{sw} = \frac{C/C_\mathrm{rand}}{L/L_\mathrm{rand}}, \tag{14}$$

and

$$\omega_\mathrm{sw} = \frac{L_\mathrm{rand}}{L} - \frac{C}{C_\mathrm{latt}}. \tag{15}$$

It is commonly recognized that "small-worldness" in a graph corresponds to $\sigma_\mathrm{sw} > 1$ and $\omega_\mathrm{sw} \approx 0$ [43, 61, 62]. Small-world network topologies are marked by high clustering and low average pathlengths, i.e., that individual "subcommunities" of nodes exist within the graph that are closely connected to each other and that particular nodes serve as highly-connected hubs bridging each subcommunity together in an efficient manner. The flow of information or impulses within these small-world networks are thus efficient with minimal loss in fidelity.

The betweenness centrality C_B of a node i serves as a metric on its hub-like connectivity, measuring the number of shortest paths between any arbitrary node pair that flows through i. For each sampled frame, the ten graph nodes with the highest normalized C_B are selected as "hubs," and the ten largest cliques are selected as the "subcommunities" of closely-connected nodes. A maximal clique for any node i is defined as the largest fully-connected subgraph containing i within the graph of interest; maximal cliques are found via the NetworkX *find_cliques()* utility and only reported if fewer than three nodes within the clique are members of an existing reported clique. In simulations where fewer than ten cliques existed, as is possible in the 125-chain HP model simulations, all independent cliques larger than a triangle (3 nodes) are reported.

6. Spatial organization within simulated condensates

To study the spatial distribution of topological features from condensate simulations, continuous trajectory samples comprising 20% of total production runs (LCD: 200 ns of 1 μs; HP sequences: $2 \times 10^7\, d\tau$ of $10^8\, d\tau$) are used, and molecular hub and clique statuses are recorded for each frame. Average radial mass density profiles are generated for each simulation to obtain phase interfaces in tandem with data on the radial distribution of hubs and cliques. In each sampled frame, all particle masses and radial distances from the dense-phase center of mass are collected and aggregated, and the mass densities are computed by radial binning. Data on the spatial localization of hubs and cliques are recorded by locating hub and clique molecules within the condensate, computing their centers of mass, determining the radial distances between molecular centers of mass and dense-phase centers of mass, and binning. Sigmoid functions are used to fit each radial mass density profile with the *scipy.optimize.curve_fit()* utility [63] to quantitatively define interfacial boundaries. The radial bounds of the interface correspond to the radial distances where the mass density is 95% and 5% of the stable dense-phase sigmoid fit value, capturing most of the region of change. Finally, distances in radial distributions are normalized by their corresponding simulation's upper (dilute-phase) interfacial boundary in order to facilitate comparison between systems.

7. Graph dynamics of the simulated condensate

To understand the time variance of topological organizations, we compute the timescales associated with the presence of hubs and cliques. The same continuous trajectory samples described in the previous section 6 are used. In each frame, the molecular indices corresponding to the ten nodes with the highest betweenness centralities and the molecular indices corresponding to the members of the 10 largest cliques are recorded. The frequency of single-molecule hub or clique status is computed as the number of frames where

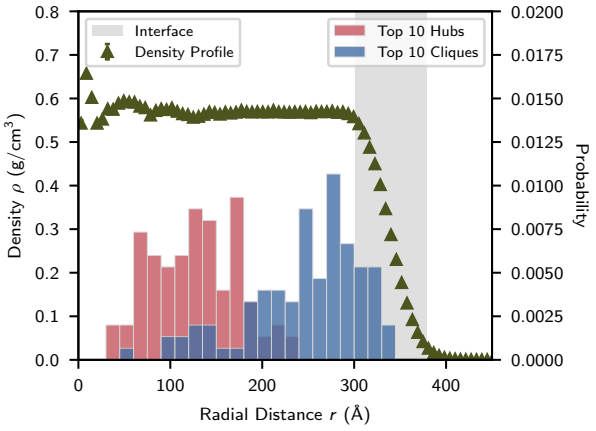

FIG. S1. Spatial distributions of hubs and cliques in a single-component FUS-LCD condensate containing 3375 chains at $T = 300$K. Consistent with results from simulations of smaller systems, clique molecules are closer to the condensate interface than hub molecules.

individual molecules are labeled as hubs or as associated with cliques, respectively. These frequencies are then normalized by the total number of sampled frames in each continuous trajectory sample.

8. Conformational analysis

To analyze the structural and conformational properties of single polymers in our simulations, we computed single-molecule radii of gyration R_g and relative shape anisotropies κ^2. These metrics are further employed to quantify changes in IDP conformational properties with respect to molecular connectivities within constructed interaction networks. Entire 1 μs or $10^8\,d\tau$ trajectories are sampled at intervals of 20 ns or $2\times10^6\,d\tau$ (i.e., every 20th frame). At each sampled frame, graph analyses are performed as described above to compute betweenness centralities C_B for each molecule. OVITO is used to obtain R_g values and diagonalized gyration tensors S for each individual molecule:

$$S = \begin{bmatrix} \lambda_1^2 & 0 & 0 \\ 0 & \lambda_2^2 & 0 \\ 0 & 0 & \lambda_3^2 \end{bmatrix}, \tag{16}$$

where eigenvalues $\lambda_1, \lambda_2, \lambda_3$ are the principal components of the molecular gyration tensor. Relative shape anisotropies κ^2 are then obtained via

$$\kappa^2 = \frac{3}{2}\frac{\lambda_1^4+\lambda_2^4+\lambda_3^4}{(\lambda_1^2+\lambda_2^2+\lambda_3^2)^2} - \frac{1}{2}, \tag{17}$$

which is bounded between 0 and 1.

9. Molecular motion through single-molecule displacement

Heterogeneities in molecular movements within condensed phases are studied by measuring single-molecule displacements at 1 ns ($10^5\,d\tau$ for HP sequences) intervals, the minimum timestep between static frames in our trajectories. As in our conformational analyses, we sample frames across trajectories of length 1 μs (or $10^8\,d\tau$) at intervals of 20 ns (or $2\times10^6\,d\tau$). For each of these frames, sampled at some timestep t, we compute the center of mass $\mathbf{r}_{i,\mathrm{COM}}(t)$ of each molecule i. The magnitudes of "instantaneous" displacements $|\Delta\mathbf{r}_i|$ are obtained by averaging the differentials of the $\mathbf{r}_{i,\mathrm{COM}}$ from frames 1 ns (or $10^5\,d\tau$) before and after the sampled frame at t, i.e., by computing $\mathbf{r}_{i,\mathrm{COM}}(t-1)$ and $\mathbf{r}_{i,\mathrm{COM}}(t+1)$, respectively:

$$\begin{aligned} |\Delta\mathbf{r}_{t,t-1}| &= |\mathbf{r}_{i,\mathrm{COM}}(t) - \mathbf{r}_{i,\mathrm{COM}}(t-1)| \\ |\Delta\mathbf{r}_{t,t+1}| &= |\mathbf{r}_{i,\mathrm{COM}}(t+1) - \mathbf{r}_{i,\mathrm{COM}}(t-1)| \\ |\Delta\mathbf{r}_i(t)| &= \frac{|\Delta\mathbf{r}_{t,t-1}| + |\Delta\mathbf{r}_{t,t+1}|}{2}. \end{aligned} \tag{18}$$

Molecular displacements $|\Delta\mathbf{r}|$ are also normalized by the length of the corresponding polymer's linear chain conformation to obtain $|\tilde{\Delta}\mathbf{r}|$ for comparison. Graph analyses are then performed to relate single-molecule displacement to molecular connectivity and topological status.

ACKNOWLEDGMENTS

The simulations reported on in this work were substantially performed using the Princeton Research Computing resources at Princeton University, which is a consortium of groups led by the Princeton Institute for Computational Science and Engineering (PICSciE) and Office of Information Technology. The authors thank Nathaniel Hess for invaluable feedback on the manuscript. The authors also thank other members of the Joseph Group for valuable discussions during various stages of manuscript preparation. D.T. acknowledges research support from the Hewlett Foundation and the New Jersey Alliance for Clinical and Translational Science (NJ ACTS), coordinated through Princeton's Office of Undergraduate Research. J.A.J. acknowledges research support from the Chan Zuckerberg Initiative DAF (an advised fund of Silicon Valley Community Foundation; grant 2023-332391), and the National Institute Of General Medical Sciences of the National Institutes of Health under Award Number R35GM155259. The content is solely the responsibility of the authors and does not necessarily represent the official views of the National Institutes of Health and other sponsors.

CONFLICT OF INTEREST

The authors declare no conflicts of interest.

DATA AVAILABILITY STATEMENT

The data supporting the findings in this study, as well as sample simulation input and output files, are available at the Joseph Group GitHub repository: https://github.com/josephresearch/LCD_Network.

[1] C. P. Brangwynne, C. R. Eckmann, D. S. Courson, A. Rybarska, C. Hoege, J. Gharakhani, F. Jülicher, and A. A. Hyman, Germline p granules are liquid droplets that localize by controlled dissolution/condensation, Science **324**, 1729 (2009).

[2] A. A. Hyman, C. A. Weber, and F. Jülicher, Liquid-liquid phase separation in biology, Annu. Rev. Cell Dev. Biol. **30**, 39 (2014).

[3] Y. Shin and C. P. Brangwynne, Liquid phase condensation in cell physiology and disease, Science **357**, eaaf4382 (2017).

[4] D. Zwicker, O. W. Paulin, and C. ter Burg, Physics of droplet regulation in biological cells, arXiv (2025).

[5] P. Li, S. Banjade, H. Cheng, S. Kim, B. Chen, L. Guo, M. Llaguno, J. V. Hollingsworth, D. S. King, S. F. Banani, P. S. Russo, Q. Jiang, B. T. Nixon, and M. K. Rosen, Phase transitions in the assembly of multivalent signalling proteins, Nature **483**, 336 (2012).

[6] R. V. Pappu, S. R. Cohen, F. Dar, M. Farag, and M. Kar, Phase transitions of associative biomacromolecules, Chem. Rev. **123**, 8945 (2023).

[7] J. P. Brady, P. J. Farber, A. Sekhar, Y.-H. Lin, R. Huang, A. Bah, T. J. Nott, H. S. Chan, A. J. Baldwin, J. D. Forman-Kay, and L. E. Kay, Structural and hydrodynamic properties of an intrinsically disordered region of a germ cell-specific protein on phase separation, PNAS **114**, E8194 (2017).

[8] J. R. Espinosa, J. A. Joseph, I. Sanchez-Burgos, A. Garaizar, D. Frenkel, and R. Collepardo-Guevara, Liquid network connectivity regulates the stability and composition of biomolecular condensates with many components, PNAS **117**, 13238 (2020).

[9] T. Mittag and R. V. Pappu, A conceptual framework for understanding phase separation and addressing open questions and challenges, Mol. Cell **82**, 2201 (2022).

[10] M. Farag, S. R. Cohen, W. M. Borcherds, A. Bremer, T. Mittag, and R. V. Pappu, Condensates formed by prion-like low-complexity domains have small-world network structures and interfaces defined by expanded conformations, Nat. Commun. **13**, 7722 (2022).

[11] F. Dar, S. R. Cohen, D. M. Mitrea, A. H. Phillips, G. Nagy, W. C. Leite, C. B. Stanley, J.-M. Choi, R. W. Kriwacki, and R. V. Pappu, Biomolecular condensates form spatially inhomogeneous network fluids, Nat. Commun. **15**, 3413 (2024).

[12] A. N. Semenov and M. Rubinstein, Thermoreversible gelation in solutions of associative polymers. 2. linear dynamics, Macromolecules **31**, 1386 (1998).

[13] M. Feric, N. Vaidya, T. S. Harmon, D. M. Mitrea, L. Zhu, T. M. Richardson, R. W. Kriwacki, R. V. Pappu, and C. P. Brangwynne, Coexisting liquid phases underlie nucleolar sub-compartments, Cell **165**, 1686 (2016).

[14] L.-P. Bergeron-Sandoval, S. Kumar, H. K. Heris, C. L. A. Chang, C. E. Cornell, S. L. Keller, P. François, A. G. Hendricks, A. J. Ehrlicher, R. V. Pappu, and S. W. Michnick, Endocytic proteins with prion-like domains form viscoelastic condensates that enable membrane remodeling, PNAS **118**, e2113789118 (2021).

[15] I. Alshareedah, M. M. Moosa, M. Pham, D. A. Potoyan, and P. R. Banerjee, Programmable viscoelasticity in protein-rna condensates with disordered sticker-spacer polypeptides, Nat. Commun. **12**, 6620 (2021).

[16] D. Michieletto and M. Marenda, Rheology and viscoelasticity of proteins and nucleic acids condensates, JACS Au **2**, 1506 (2022).

[17] I. Alshareedah, W. M. Borcherds, S. R. Cohen, A. Singh, A. E. Posey, M. Farag, A. Bremer, G. W. Strout, D. T. Tomares, R. V. Pappu, T. Mittag, and P. R. Banerjee, Sequence-specific interactions determine viscoelasticity and ageing dynamics of protein condensates, Nat. Phys. **20**, 1482 (2024).

[18] D. Aierken and J. A. Joseph, Accelerated simulations reveal physicochemical factors governing stability and composition of rna clusters, J. Chem. Theory Comput. **20**, 10209 (2024).

[19] Y. Shen, A. Chen, W. Wang, Y. Shen, F. S. Ruggeri, S. Aime, Z. Wang, S. Qamar, J. R. Espinosa, A. Garaizar, P. St George-Hyslop, R. Collepardo-Guevara, D. A. Weitz, D. Vigolo, and T. P. J. Knowles, The liquid-to-solid transition of fus is promoted by the condensate surface, PNAS **120**, e2301366120 (2023).

[20] C. He, C. Y. Wu, W. Li, and K. Xu, Multidimensional super-resolution microscopy unveils nanoscale surface aggregates in the aging (milano) of fus condensates, J. Am. Chem. Soc. **145**, 24240 (2023).

[21] A. Garaizar, J. R. Espinosa, J. A. Joseph, G. Krainer, Y. Shen, T. P. J. Knowles, and R. Collepardo-Guevara, Aging can transform single-component protein condensates into multiphase architectures, PNAS **119**, e2119800119 (2022).

[22] W. Borcherds, A. Bremer, M. B. Borgia, and T. Mittag, How do intrinsically disordered protein regions encode a driving force for liquid–liquid phase separation?, Curr. Opin. Struct. Biol. **67**, 41 (2021).

[23] J. Wang, J. M. Choi, A. S. Holehouse, H. O. Lee, X. Zhang, M. Jahnel, S. Maharana, R. Lemaitre, A. Pozniakovsky, D. Drechsel, I. Poser, R. V. Pappu, S. Alberti, and A. A. Hyman, A molecular grammar underlying the driving forces for phase separation of prion-like rna-binding proteins, Cell **174**, 688 (2018).

[24] A. Bremer, M. Farag, W. M. Borcherds, I. Peran, E. W. Martin, R. V. Pappu, and T. Mittag, Deciphering how naturally occurring sequence features impact the phase behaviours of disordered prion-like domains, Nat. Chem. **14**, 196 (2022).

[25] E. W. Martin, A. S. Holehouse, I. Peran, M. Farag, J. J. Incicco, A. Bremer, C. R. Grace, A. Soranno, R. V. Pappu, and T. Mittag, Valence and patterning of aromatic residues determine the phase behavior of prion-like domains, Science **367**, 694 (2020).

[26] A. N. Semenov and M. Rubinstein, Thermoreversible gelation in solutions of associative polymers. 1. statics, Macromolecules **31**, 1373 (1998).

[27] M. J. Maristany, A. A. Gonzalez, J. R. Espinosa, J. Huertas, R. Collepardo-Guevara, and J. A. Joseph, Decoding phase separation of prion-like domains through data-driven scaling laws, eLife **13**, RP99068 (2025).

[28] L. M. Jawerth, M. Ijavi, M. Ruer, S. Saha, M. Jahnel, A. A. Hyman, F. Jülicher, and E. Fischer-Friedrich, Salt-dependent rheology and surface tension of protein condensates using optical traps, Phys. Rev. Lett. **121**, 258101 (2018).

[29] D. Sundaravadivelu Devarajan and J. Mittal, Sequence-encoded spatiotemporal dependence of viscoelasticity of protein condensates using computational microrheology, JACS Au **4**, 4394 (2024).

[30] T. Wu, M. R. King, Y. Qiu, M. Farag, R. V. Pappu, and M. D. Lew, Single-fluorogen imaging reveals distinct environmental and structural features of biomolecular condensates, Nat. Phys. (2025).

[31] Z.-S. Yan, Y.-Q. Ma, and H.-M. Ding, Unveiling the multicomponent phase separation through molecular dynamics simulation and graph theory, J. Chem. Phys. **160** (2024).

[32] J. C. Shillcock, C. Lagisquet, J. Alexandre, L. Vuillon, and J. H. Ipsen, Model biomolecular condensates have heterogeneous structure quantitatively dependent on the interaction profile of their constituent macromolecules, Soft Matter **18**, 6674 (2022).

[33] J. Wang, D. S. Devarajan, A. Nikoubashman, and J. Mittal, Conformational properties of polymers at droplet interfaces as model systems for disordered proteins, ACS Macro Lett. **12**, 1472 (2023).

[34] J. Wang, D. S. Devarajan, K. Muthukumar, Y. C. Kim, A. Nikoubashman, and J. Mittal, Sequence-dependent conformational transitions of disordered proteins during condensation, Chem. Sci. **15**, 20056 (2024).

[35] D. S. Devarajan, J. Wang, B. Szała-Mendyk, S. Rekhi, A. Nikoubashman, Y. C. Kim, and J. Mittal, Sequence-dependent material properties of biomolecular condensates and their relation to dilute phase conformations, Nat. Commun. **15**, 1912 (2024).

[36] D. J. Bauer and A. Nikoubashman, The conformations of protein chains at the interface of biomolecular condensates, Nat. Commun. **15**, 9975 (2024).

[37] O. Sporns and J. D. Zwi, The small world of the cerebral cortex, Neuroinformatics **2**, 145 (2004).

[38] D. Watts and S. Strogatz, Collective Dynamics of Small-World Networks, Nature **393**, 440 (1998).

[39] J. A. Joseph, A. Reinhardt, A. Aguirre, P. Y. Chew, K. O. Russell, J. R. Espinosa, A. Garaizar, and R. Collepardo-Guevara, Physics-driven coarse-grained model for biomolecular phase separation with near-quantitative accuracy, Nat. Comp. Sci. **1**, 732 (2021).

[40] L. Emmanouilidis, E. Bartalucci, , Y. Kan, M. Ijavi, M. E. Pérez, P. Afanasyev, D. Boehringer, J. Zehnder, S. H. Parekh, M. Bonn, T. C. T. Michaels, T. Wiegand, and F. H.-T. Allain, A solid beta-sheet structure is formed at the surface of fus droplets during aging, Nat. Chem. Bio. **20**, 1044 (2024).

[41] A. Statt, H. Casademunt, C. P. Brangwynne, and A. Z. Panagiotopoulos, Model for disordered proteins with strongly sequence-dependent liquid phase behavior, J. Chem. Phys. **152** (2020).

[42] D. J. Watts, *Small Worlds* (Princeton University Press, Princeton, NJ, 1999).

[43] Q. K. Telesford, K. E. Joyce, S. Hayasaka, J. H. Burdette, and P. J. Laurienti, The ubiquity of small-world networks, Brain Connect. **1**, 367 (2001).

[44] S. P. O. Danielsen, A. N. Semenov, and M. Rubinstein, Phase separation and gelation in solutions and blends of heteroassociative polymers, Macromolecules **56**, 5661 (2023).

[45] M. Newman, *Networks* (Oxford University Press, 2018).

[46] D. N. Theodorou and U. W. Suter, Shape of unperturbed linear polymers: polypropylene, Macromolecules **18**, 1206 (1985).

[47] H. Arkın and W. Janke, Gyration tensor based analysis of the shapes of polymer chains in an attractive spherical cage, J. Chem. Phys. **138** (2013).

[48] D. Aierken and M. Bachmann, Impact of bending stiffness on ground-state conformations for semiflexible polymers, J. Chem. Phys. **158** (2023).

[49] K. A. Burke, A. M. Janke, C. L. Rhine, and N. L. Fawzi, Residue-by-residue view of in vitro fus granules that bind the c-terminal domain of rna polymerase ii, Mol. Cell **60**, 231 (2015).

[50] W. Zheng, G. L. Dignon, N. Jovic, X. Xu, R. M. Regy, N. L. Fawzi, Y. C. Kim, R. B. Best, and J. Mittal, Molecular details of protein condensates probed by microsecond long atomistic simulations, J. Phys. Chem. B **124**, 11671 (2020).

[51] G. Gao, E. R. Sumrall, and N. G. Walter, Single molecule tracking reveals nanodomains in biomolecular condensates, bioRxiv (2024).

[52] N. Hess and J. A. Joseph, Structured protein domains enter the spotlight: modulators of biomolecular condensate form and function, Trends Biochem. Sci. (2025).

[53] C. Dollinger, E. Potolitsyna, A. G. Martin, A. Anand, G. K. Datar, J. D. Schmit, and J. A. Riback, Nanometer condensate organization in live cells derived from partitioning measurements, bioRxiv (2025).

[54] D. Aierken, V. Zhang, R. Sealfon, J. C. Marecki, K. D. Raney, A. S. Gladfelter, J. A. Joseph, and C. A. Roden, Biomolecular condensates control and are defined by rna-rna interactions that arise in viral replication, bioRxiv (2024).

[55] X. Wang, S. Ramírez-Hinestrosa, J. Dobnikar, and D. Frenkel, The lennard-jones potential: when (not) to use it, Phys. Chem. Chem. Phys. **22**, 10624 (2020).

[56] J. M. Lotthammer, G. M. Ginell, D. Griffith, R. Emenecker, and A. S. Holehouse, Direct prediction of intrinsically disordered protein conformational properties from sequence, Nat. Methods **21**, 456 (2024).

[57] K. Kremer and G. S. Grest, Dynamics of entangled linear polymer melts: A molecular-dynamics simulation, J. Chem. Phys. **92**, 5057 (1990).

[58] A. P. Thompson, H. M. Aktulga, R. Berger, D. S. Bolintineanu, W. M. Brown, P. S. Crozier, P. J. in 't Veld, A. Kohlmeyer, S. G. Moore, T. D. Nguyen, R. Shan, M. J. Stevens, J. Tranchida, C. Trott, and S. J. Plimpton, LAMMPS - a flexible simulation tool for particle-based materials modeling at the atomic, meso, and continuum scales, Comp. Phys. Comm. **271**, 108171 (2022).

[59] A. Stukowski, Visualization and analysis of atomistic simulation data with OVITO-the Open Visualization Tool, Model. Simul. Mater. Sci. Eng. **18** (2010).

[60] A. A. Hagberg, D. A. Schult, and P. J. Swart, Exploring network structure, dynamics, and function using networkx, in *Proceedings of the 7th Python in Science Conference*, edited by G. Varoquaux, T. Vaught, and J. Millman (Pasadena, CA USA, 2008) pp. 11 – 15.

[61] M. D. Humphries, K. Gurney, and T. J. Prescott, The brainstem reticular formation is a small-world, not scale-free, network, Proc. R. Soc. B **273**, 503 (2006).

[62] M. D. Humphries and K. Gurney, Network 'small-world-ness': A quantitative method for determining canonical network equivalence, PLoS One **3**, e0002051 (2008).

[63] P. Virtanen, R. Gommers, T. E. Oliphant, M. Haberland, T. Reddy, D. Cournapeau, E. Burovski, P. Peterson, W. Weckesser, J. Bright, S. J. van der Walt, M. Brett, J. Wilson, K. J. Millman, N. Mayorov, A. R. J. Nelson, E. Jones, R. Kern, E. Larson, C. J. Carey, İ. Polat, Y. Feng, E. W. Moore, J. VanderPlas, D. Laxalde, J. Perktold, R. Cimrman, I. Henriksen, E. A. Quintero, C. R. Harris, A. M. Archibald, A. H. Ribeiro, F. Pedregosa, P. van Mulbregt, and SciPy 1.0 Contributors, SciPy 1.0: Fundamental Algorithms for Scientific Computing in Python, Nat. Methods **17**, 261 (2020).